energy&fuels

Article

pubs.acs.org/EF

Prediction of Potassium Chloride Sulfation and Its Effect on Deposition in Biomass-Fired Boilers

M. U. Garba,[†] D. B. Ingham,[†] L. Ma,*[,†] R. T. J. Porter,[†] M. Pourkashnian,[†] H. Z. Tan,[‡] and Alan Williams[†]

[†]Energy Technology and Innovation Initiative (ETII), Faculty of Engineering, University of Leeds, Leeds LS2 9JT, United Kingdom

[‡]Key Laboratory of Thermo-Fluid Science and Engineering, Ministry of Education, Xian Jiaotong University, Xi'an 710049, China

ABSTRACT: In this paper, a model that couples a reduced alkali kinetic mechanism for alkali sulfate formation during biomass combustion with an ash deposition model using computational fluid dynamics (CFD) techniques is presented. Starting with a detailed gas-phase kinetic mechanism for alkali chemistry, a systematic reduction procedure has been performed using sensitivity analysis to reduce the reaction mechanism to a level that can be implemented into a CFD calculation. This reduced mechanism has been validated against the full reaction mechanism under the temperature conditions that typically occur in biomass combustion furnaces. Both mechanisms are compared to the experimental data obtained using a plug flow reactor reported in the literature. An ash deposition model taking into considerations the ash-sticking probability and the condensation of potassium salts has been developed. The reduced mechanism and the deposition model developed are implemented into a CFD model to predict ash depositions in a 10 MW_{th} biomass grate furnace. The model has adequately reproduced the deposit position and shape as observed in the test furnace.

1. INTRODUCTION

Cotton straw is a readily available agriculture waste product, and it is widely used as a renewable energy source. About 600 million tons of straws and stalks are produced annually[1] in China, and 17.8 million tons are produced annually in the U.K.[2] Direct combustion of straw in grate furnaces is mainly used, but there are great problems with slagging and fouling. This is because cotton straw contains large amounts of potassium, chlorine, and silicon, which often lead to a rapid buildup of unmanageable amounts of deposits, resulting in reduced boiler efficiency and unscheduled plant shutdown.

In biomass combustion, generally, the main part of the deposit is formed by particle inertial impaction, but other deposition phenomena, such as chemical reaction and condensation, are also of great importance with regard to deposition of potassium, chlorine, and sulfur. Sulfation of potassium hydroxide and potassium chloride are important chemical reactions that lead to ash deposition in both coal and biomass combustion. Alkali compounds contained in the fuel may be released during combustion and form alkali species, including salts and particulate matter (fly ash particles and aerosols). Under grate-firing conditions, particles of different sizes are characterized into two main groups: fine particles that usually consist of aerosols with diameters between 30 and 300 nm and coarse particles that mainly consist of nonvolatilized ash residuals with diameters between 1 and 100 μm, depending upon the fuel and furnace.[28] Deposition of the sub-micrometer class of particles is mainly influenced by the thermophoresis and turbulent diffusion within the turbulent boundary layer. Deposition of larger fly ash particles is more likely to be dictated by the inertial impaction. In this paper, the particle sizes up to approximately 110 μm have been considered on the basis of experimental data from combustion of waste wood and wood chips.[28]

There is still a lack of knowledge on the exact mechanism of potassium release during biomass combustion, particularly when the particle is being heated at a high rate and to a high temperature, as found in grate-fired furnaces. It is generally accepted that the release of potassium from biomass particles is usually in the form of KCl and/or KOH, depending upon the biomass composition. The former, in particular, is among the most stable high-temperature, gas-phase, alkali-containing species. The chlorine content in the biomass often dictates the amount of potassium release during combustion, and it also strongly influences the transport of alkali from the fuel to heating tube surfaces, where the alkali often forms sulfates. The potassium that is released into the gas flow undergoes complex transformation and forms KOH, KCl, and K_2SO_4 in different temperature regimes. They are expected to nucleate as well as form aerosols in the flue gas. KCl and K_2SO_4 can condense on the surfaces of the fly ash/aerosols and on the superheater system, thus providing a sticking layer for the arriving particles to deposit.[4−7]

The reactions between the alkali and sulfate have only been investigated to a certain extent.[8−12] Several authors have reported the properties of fine alkali particles emitted from biomass-fired furnaces.[10−14] These particles are found to consist of alkali chlorides and sulfates in relative amounts that depend upon not only the properties of the fuels burned but also the characteristics of the boiler.[11,12] Christensen et al.[11] developed a model for the formation of fine particles during the combustion of straw. They deduced that the oxidation of SO_2 to SO_3 was the rate-limiting reaction in the formation of

Special Issue: International Conference on Carbon Reduction Technologies

Received: October 28, 2011
Revised: January 12, 2012
Published: February 3, 2012

alkali sulfate. Further investigation by these authors in laboratory experiments with different biomasses confirmed this limiting step.[13] Recently, Glarborg and Marshal[7] proposed a detailed reaction mechanism for gaseous alkali formation in combustion conditions, and the model adequately reproduced some experimental results on sulfation of gaseous KCl. According to the detailed mechanism,[7] the modeling of the formation of alkali sulfates from alkali chlorides, found in deposits or ash particles, is based on the assumption that potassium species first transform in the gas phase (homogeneous reactions) and then react in condensed or solid phases (heterogeneous reactions). In a proposed heterogeneous mechanism, a gas-phase alkali-containing precursor is transported to a surface where it is then sulfated by reactions in condensed or solid phases. Concerning the homogeneous reaction, alkali sulfate aerosol seeds are formed in a series of steps occurring in the gas phase by homogeneous nucleation. The seeds also act as condensation nuclei for further condensation of alkali sulfate vapors and other supersaturated vapors, e.g., alkali chlorides, as the flue gas cools.[7,8,14] Iisa et al.[15] provide detailed measurements of the rate of sulfation of KCl in gas and condensed phases and demonstrated that the rate of sulfation is considerably slower in the condensed phase.

Previous numerical studies have addressed deposition on heat-exchange surfaces as a function of tube arrangements,[16] locations within the boiler,[3,17] and deposition probe location.[18] Most of these studies have focused on the modeling of particle-sticking behavior, such as ash particle viscosity and melting fraction, to determine the particle collection efficiency.[3,4,19−21] The size of fly ash adhered together by alkali salts is also essential in determining the sticking probability. The effects of this factor have been investigated in coal combustion,[22] but in biomass combustion, which has a higher content of inorganic components and more interactions and association of these elements, little has been reported. The ash-forming vapor is involved in a complex system. Because of the strong dependence of the kinetic rates upon the temperature,[11] it is expected that the composition of ash-forming vapors will be near equilibrium conditions at typical flame temperatures, with increasing deviation from equilibrium at lower temperatures, as the flue gas cools and condenses on the heat-transfer surfaces. As a result of this condensation, high concentrations of K, Cl, and S constitute the initial deposit. The aim of this paper is to reduce a comprehensive alkali mechanism for the sulfation of KCl to a level that may be practically implemented into computational fluid dynamics (CFD) simulations of alkali species transformation in a combustion system and to implement the reduced mechanism in a test furnace to determine its effect on the initial deposit formation incorporating an ash deposition model. The organization of this paper is as follows. Section 2 outlines the two main stages of the research, i.e., (i) development of a reduced mechanism from a detailed alkali mechanism and (ii) development of an ash deposition model taking into consideration the ash-sticking probability and the condensation of potassium salts. In section 3, the reduced reaction mechanism and the deposition model developed are combined in a CFD model to simulate the initial stage of deposit buildup in a 10 MW industrial test furnace. The results of model validations and predictions are presented and discussed together with relevant experimental data.

2. NUMERICAL MODELS

2.1. Overview of the Scheme. The interaction between the involved chemical reactions within the turbulent reactive flow, species condensation, nucleation, and deposition of ash particles is very complicated in nature.[23] For biomass with a high content of chlorine in the fuel mix, such as cotton straw that is being investigated in this work, sulfation of KCl is a dominant pathway.[10] The presence of KOH in the gas phase is stable at higher temperatures and with a high content of water vapor (H_2O) and a low content of Cl.[12] In the post-combustion region, the flue gas meets with the superheaters and it cools. When the saturation pressure of KCl and K_2SO_4 is reached, they can condense and deposit on cooled surfaces. Condensation can occur either by direct condensation on the tube surface, on fly ash particles, or by forming aerosols in the free gas stream within the thermal boundary layer close to the surface, as depicted in Figure 1.[4]

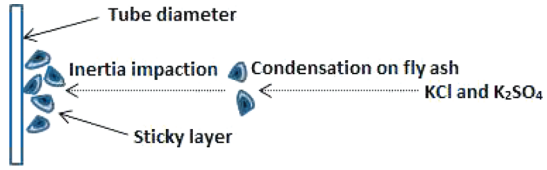

Figure 1. Systematic presentation of vapor deposition.[4]

The formation of KCl and K_2SO_4 involves H_2/O_2, chlorine, sulfur, potassium, and the interactions between them.[7,8] The implementation of a detailed alkali reaction mechanism in a multi-dimensional and large-scale CFD calculation is computationally expensive, often even prohibitive, and therefore, developing a reduced alkali mechanism is a necessary precondition. The approach taken in this investigation was to remove redundant species and reactions from the detailed reaction mechanism using sensitivity analysis at specified reaction conditions that are pertinent to the grate furnace combustion investigated. Once the reduced mechanism has been developed, it is validated against both experimental data and the detailed reaction mechanism from which it was reduced to ensure that any performance error incurred as a result of the reduction is within an acceptable level. The reduced mechanism is then imported into the CFD model in the CHEMKIN format and is used to calculate the production and destruction of the species participating in the chemical reactions.[24,25] The condensation of alkali salts in the flue gas is addressed as a reaction step that is added to the reaction mechanism with the rate constant suggested by Glarborg and Marshal.[8] An ash deposition model is developed principally on the basis of the modeling concept suggested by Tomeczek et al.[16,22] for calculating the deposition of ash on the furnace wall and heat-exchange surfaces. The model takes into consideration the contributions from both the condensation of alkali salts and the ash loading in the flue gas stream. The predicted species concentration and other parameters of the flue gas flow from the CFD calculations are fed into the deposition model for the prediction of deposition.

2.2. Reduction of the Detailed Alkali Mechanism. To produce a reduced alkali mechanism that retains the essential features of the detailed chemistry but with much improved computational efficiency in terms of computer memory usage and central processing unit (CPU) time, we start with the detailed chemical kinetic model by Hindiyarti et al.[8] that includes 54 chemical species and 220 elementary steps. A systematic reduction procedure based on a sensitivity analysis was performed to remove redundant chemical species and reactions from the detailed mechanism using the KINALC software code.[25,26] The code is a post-processor to the CHEMKIN family of codes that are used to integrate the governing coupled differential equations that describe the rate of change of the gas concentration for each chemical species in a given reactor with highly simplified physics.

2.3. Deposition Model. The formation of deposits on heat-transfer surfaces during biomass combustion is a complex phenomena that depends upon (a) transformation of the inorganic components of ash in fuels, (b) chemical reactions between the gas, liquid, and solid

dx.doi.org/10.1021/ef201681t | Energy Fuels 2012, 26, 6501−6508

phases in suspension and on surfaces, (c) reaction kinetics and species transport, and (d) attachment of ash particles to surfaces and the release of deposited liquids and solids.[23] Thus, it is evident that deposition problems cannot be resolved by a single rate of deposition on a surface. The deposit formation pathways in power plant furnaces include inertia impaction, effect of thermophoresis, turbulent diffusion, chemical reactions, and condensation of alkali salts. Inertia (particles larger than 10 μm) and thermophoresis (particles smaller than 10 μm) involve a solid phase. Condensation and chemical reactions affect the gas phase. Turbulence diffusion can have an effect on the transport of solid, liquid, and gaseous phases near the heating surface but have a stronger effect on the movement of sub-micrometer particles. In terms of chemical reactions, the most important reactions that lead to deposition are sulfation, silica absorption, and oxidation. In particular, sulfation of supersaturated vapors, such as KCl and K_2SO_4 chlorides, enhances deposition.[9,10]

The primary source of ash deposition on superheater boiler tubes is by impaction, while condensation of potassium species plays a crucial or even dominant role[1,4] on retaining the incoming ash particles on the deposit surface. In the downstream section of the boiler, where the flue gas is sufficiently cooled within the boundary layer of the superheater tubes, as is the situation investigated in this paper, the alkali salts as well as the fly ash particles will condense and stick on the tube surface. Tomeczek et al.[16,22] proposed a concept of particle-size-dependent ash-sticking probability and assumed it to be equal to the product of the estimated deposition rate coefficient, S, based on the final deposit size formed on the superheater and the flux of vapors condensing on its unit surface area and forming a sticky layer, $m_{c,A}$. Therefore, particle sticking probability, P, can be expressed as follows:

$$P = Sm_{c,A} \tag{1}$$

The estimated deposition rate coefficient S = 56 $(\mathrm{kg\ m^{-2}\ s^{-1}})^{-1}$ has been used in this paper, and this is based on the deposit formed during a 3 day uninterrupted onsite experiment on a single vertical secondary superheater.[16,22] The flux of ash vapors condensing on the fly ash within the tube boundary layer, diffusing toward a unit surface area of tube surface, and condensing later on it can be calculated by

$$m_{c,A} = Shd_p^2 \frac{C_p}{C_{t,p}} D_i \left(\frac{p_i - p_{s,i}}{kT_p} \right) \rho_g \tag{2}$$

where C_p is the concentration of the fly ash particles, $d_p > 1$ μm, within the boundary layer where ash-forming vapor condenses on the fly ash particle, $C_{t,p}$ is the total concentration of fly ash particles,[28] p_i is the partial pressure of the ith gaseous component, $p_{s,i}$ is the saturation pressure of the ith gaseous salt component, Sh is the Sherwood number, T_p is the particle temperature, k is Boltzmann's constant, and ρ_g is the flue gas density. The diffusion coefficients of KCl and K_2SO_4 condensing on the fly ash particle are defined as a function of the flue gas temperature: $D_{KCl} = 2.67 \times 10^{-9} T_f^{2/3}$ and $D_{K_2SO_4} = 1.78 \times 10^{-9} T_f^{2/3}$.[29] The particles are assumed to take a spherical shape, and d_p is the diameter of the particle. Following Tomeczek et al.,[22] the saturation pressure for potassium salts considered is calculated as follows:

$$p_{s,i} = p_n \exp(A_i - B_i/(T_f + C_i)) \tag{3}$$

where A_i, B_i, and C_i are constants given in Table 1, $p_n = 10^5$ Pa, and T_f is the local gas temperature.

Table 1. Constants A_i, B_i, and C_i in eq 3

component	A_i	B_i (K)	C_i (K)	temperature range (K)
K_2SO_4	18.08	39449	0	1150−1800
KCl	11.01	17132	−122.7	1094−1680

The deposition flux of a single particle that hits the tube can be evaluated from the mass flux of the particles, denoted by their trajectories, $m_{trj,i}$, and the sticking probability of the impacting particle, P. The total deposition flux on the tube unit surface area can be determined by[17]

$$\dot{m} = \sum_{i=0}^{n} (m_{trj,i} P) \tag{4}$$

The model used[22] in this paper was originally developed for coal combustion but allows for the inclusion of alkali salt species. Thus, it was considered to be suitable for biomass combustion.

2.4. Inclusion into the CFD Models. The commercially available CFD software package FLUENT 12.1[27] was used in this paper. FLUENT solves the Favre-averaged form of the governing equations, including a set of chemical species transport equations. The reduced alkali mechanism developed, together with all of the thermodynamic properties that are required, is imported into the CFD model in a typical CHEMKIN format, where it is used to calculate the production and destruction term in the transport equations for the chemical species. Typical solutions from a CFD code include temperature, pressure, velocity, and species concentration of the fluid in the computational domain. With solid fuel combustion, the transport of fuel/ash particles in the computational domain is typically calculated using the Lagrangian frame of reference. Therefore, the tracking of particles through the furnace and the angle at which the particles hit a wall surface is calculated using CFD. The ash deposition model is integrated into the CFD model using user-defined function (UDF) DEFINE_DPM_EROSION. The variables required in the deposition model include the partial pressure, saturation pressure, diffusion coefficient of K_2SO_4, and information on the ash particles. They are all part of the solution of the CFD solver and are used as input to the ash deposition model. The ash deposition calculation may be performed as a post-process after the reacting flow simulation is complete if the impact of the ash buildup on the heat transfer and fluid flow is ignored, as may be the case in the initial stages of ash deposition.

3. VALIDATION OF THE ALKALI REACTION MECHANISM

3.1. Detailed Mechanism Validation. To investigate and later validate both the detailed and reduced alkali mechanisms, the experimental data by Iisa et al.[15] was chosen for model evaluation. It was conducted under well-controlled conditions that are within the temperature regime of a typical biomass combustion flue gas. The experiments employed a laminar entrained flow reactor, where small, solid particles (65−125 μm) of KCl are fed at a rate of 0.24 g/min, together with a gaseous mixture containing 2% SO_2, 5% O_2, 10% H_2O, and N_2. The particles were rapidly heated at 1173−1373 K by hot reactor walls and the hot secondary gas with a residence time of up to 1.5 s. The heated KCl particles became molten, partially vaporized, and then became sulfated in the presence of SO_2, O_2, and H_2O. The products of the reaction between the vapor phase (i.e., SO_2, O_2, and H_2O) and molten KCl were collected separately and analyzed for ions of K, SO_4, and Cl using capillary electrophoresis analysis to determine the extent of alkali sulfation. It should be noted that these solid KCl particles are employed purely for the purpose of producing gas-phase KCl in the entrained flow reactor to investigate the alkali sulfation. They are not used for particle deposition experiments.

The evaporation of the solid potassium chloride was modeled with three pseudo-first-order reactions taken from ref 8, with rate constants fitted to match the experimental data in the detailed mechanism. Figures 2 and 3 show the predicted KCl vaporization and sulfation as a function of the residence time from the full alkali mechanism, and they are compared to the experimental data obtained from the entrained flow reactor at 1373 K. It is observed that the prediction of KCl vaporization and sulfation by the detailed mechanism are in good agreement,

dx.doi.org/10.1021/ef201681t | Energy Fuels 2012, 26, 6501−6508

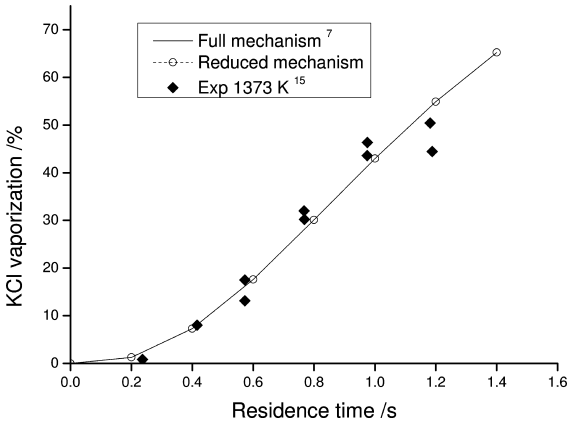

Figure 2. Vaporization of KCl as a function of the residence time at 1373 K.

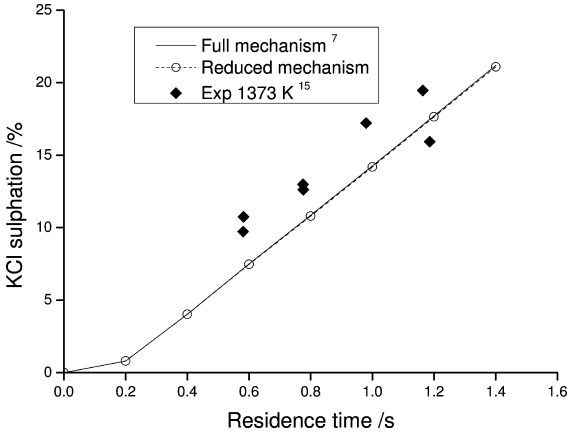

Figure 3. Conversion of KCl to K_2SO_4 as a function of the residence time at 1373 K.

although the theoretical simulation of sulfation of KCl slightly underpredicts the experimental data. Similar observations with respect to the underprediction were also reported for the detailed mechanism in the work by Hindiyarti et al.[8]

3.2. Reduced Mechanism. The reduced mechanism was developed through the iterative analysis of the Jacobian matrix[25,26] of the system of kinetic differentials that investigates the effect of species concentration changes on the rates of production of important and necessary species. The aim of the reduction is to produce a reduced subset of species and reactions that can reproduce the concentrations of important species or important reaction features that are represented in the detailed mechanism. Thresholds for ranked species sensitivities were applied at several predicted biomass post-combustion reaction conditions, and the union of necessary species over these conditions was taken. As a result, a reduced mechanism comprising 36 species, i.e., SO_2, SO_3, K, KO, KO_2, KOH, $K_2O_2H_2$, KCl, K_2Cl_2, $KHSO_3$, KSO_4, KSO_2, KSO_3, $KHSO_4$, K_2SO_4, KSO_3Cl, $K_2SO_4[B]$, CO, CO_2, H, O, OH, H_2, O_2, HO_2, H_2O, H_2O_2, HOSO, $HOSO_2$, HCl, Cl_2, Cl, ClO, HOCl, ClOO, and N_2, and 137 reversible reactions was created. The validation of the reduced mechanism is performed by a comparison to the benchmark performance of the full mechanism and the experimental data from the entrained flow reactor, as shown in Figures 2 and 3.

Examination of the features of the reduced mechanism reveals that the potassium vaporization process is well-predicted by the reduced scheme (see Figure 2), where the two theoretical predictions overlap each other. In terms of the KCl sulfation predictions shown in Figure 3, the predictions obtained using the reduced mechanism are shown to reproduce the primary features of the detailed mechanism and they almost overlap each other. It may be concluded that the reduced alkali mechanism with 36 species and 137 reactions can reproduce the predictions from the full detailed reaction mechanism under the conditions investigated. This corresponds to a computational cost reduction of at least 50%. It is possible to reduce the numbers of species and reactions even further. However, the increased error induced by the reduction below the 36 necessary species and 137 reversible reactions was considered to be unsatisfactory, and it gave little extra computational saving.

4. PREDICTION OF DEPOSITION IN A GRATE FURNACE

To investigate the capabilities of the model developed to predict the effect of condensable alkali salts on ash deposition rates, simulations were performed for a 10 MW_{th} biomass-fired industrial grate furnace. A complete modeling of a biomass-fired grate boiler involves the modeling of biomass combustion inside the fuel bed on the grate and gas-phase reaction above the grate bed (freeboard). The coupling of the two processes has been modeled by several investigators, taking into considerations the combustion gas released from the fuel bed into the freeboard and the radiative heat flux emitted by the flame and furnace walls onto the fuel bed.[32] However, for the purpose of investigating ash depositions on the superheaters downstream of the boiler, in this paper, only the second half of the entire boiler was simulated, with the boundary conditions enforced on the model being obtained from the onsite measurements.

The boiler uses an M-type arrangement and four grate superheaters, as is schematically shown in Figure 4. The flue gas

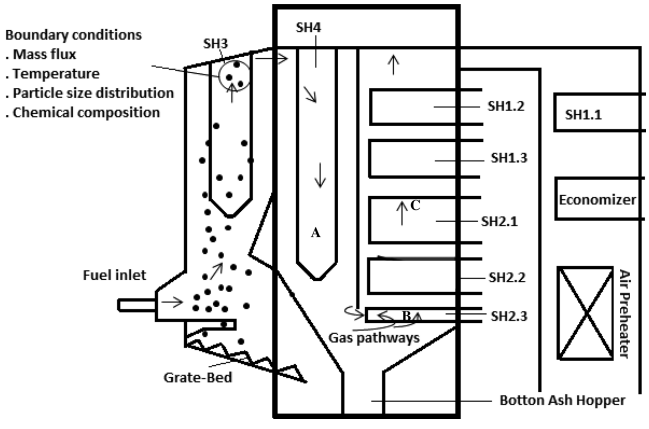

Figure 4. Schematic diagram of the Shenyang power plant furnace.[34]

leaves the furnace through the third (SH3), fourth (SH4), secondary (SH2), and then primary (SH1) superheaters one after the other and then goes through the economizer and the air preheater. Heavy slag formed on the furnace is found in the cooler section of the boiler where the fourth, secondary, and primary superheaters[34] are located. The locations correspond to the section where combustion gases deviate from being in equilibrium and the kinetic dependence upon temperature becomes significant. Cotton straw is used as the fuel in the

dx.doi.org/10.1021/ef201681t | Energy Fuels 2012, 26, 6501–6508

experiments, and its typical chemical and thermophysical properties as found experimentally and used as input to the simulation are shown in Table 2. As expected, a high level of K and Cl is present in the fuel analytic data. A more detailed description of the furnace and the experiments performed can be found in the study by Niu et al.[34]

Table 2. Chemical and Thermophysical Properties of the Cotton Straw (wt %)

proximate analysis (wt %, as received)		physical property of the fuel	
moisture	2.63	density (kg/m^3)	570
ash	4.22	specific heat (J kg^{-1} K^{-1})	1670
volatile matter	72.61	heat conductivity (W m^{-1} K^{-1})	0.12
fixed carbon	20.54		
ultimate analysis (wt %, as received)		ash (wt %, as received)	
C	45.86	SiO_2	13.74
H	5.53	Al_2O_3	4.03
O	40.96	Fe_2O_3	1.16
N	0.61	CaO	25.15
S	0.19	MgO	10.99
Cl	0.44	TiO_2	0.21
K	1.03	SO_3	5.75
		P_2O_5	6.98
		K_2O	25.40
		Na_2O	6.58

4.1. CFD Model. The section of the boiler considered for the deposit formation simulations is indicated as enclosed in a thick box in Figure 4. As mentioned previously, only half of the boiler is considered in the CFD model, which covers all of the locations where deposits are formed on the superheaters. The main dimensions used in the CFD model are indicated in Figure 5a. The diameter of the tube use in the superheaters is 38 mm. Further, the computational domain is meshed with the GAMBIT mesh generator, and the mesh employed consists initially of about 1 million cells. The grid was later continuously refined to ensure a grid-independent solution, which ended up with 1.9 million cells. No significant change in the gas temperature and the velocity distribution with a further increase in the number of computational cells was observed. A typical computational mesh is shown in Figure 5b.

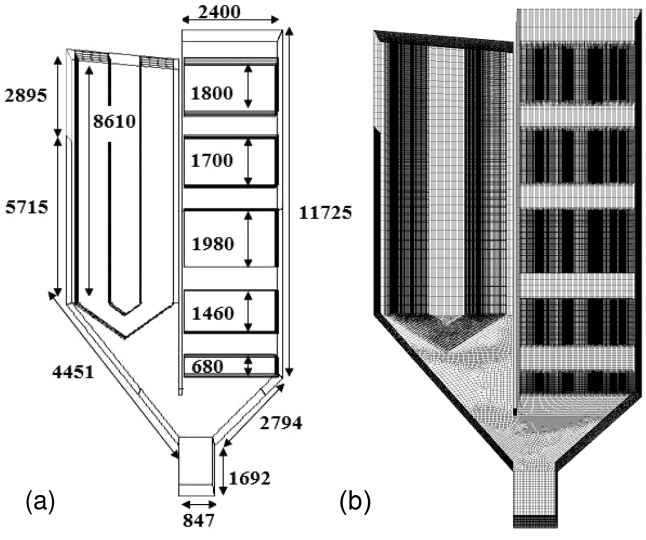

Figure 5. (a) Schematic diagram of the CFD model with dimensions (in millimeters) included and (b) computational grid.

All of the boundary conditions used for the CFD model are taken from experimental data and/or theoretical estimations. For simplicity, a mean flow rate at the inlet of the computational domain of 10 kg/s of flue gas is applied over the entire boiler inlet area with a temperature of 1274 K. In the absence of experimental data, the ash particle size distribution obtained from the combustion of waste wood and wood chips[28,36] has been used ranging from approximately 1 to 110 μm, as shown in Table 3. Immediately downstream from the combustion zone it is likely that the gas phase quickly reaches and maintains equilibrium because of the high temperature.[13] Therefore, chemical equilibrium is assumed at the inlet of the computational domain. Then, the chemical species concentrations, as shown in Table 4 and the fractions of gas, liquid, and solid phases in the flue gas are estimated using FactStage thermoequilibrium calculations based on the composition of the fuel cotton straw.[33] Average superheater tube temperatures of 764, 731, and 663 K were used on the basis of the steam temperature of the fourth, secondary, and primary superheaters, respectively. The steam temperature is approximately 650 K at the exit of the primary superheater. The furnace wall temperature is specified between 600 and 1000 K based on the estimated local water tube surface temperature.

Table 3. Size Class for Fly Ash Distribution

size class	particle concentration (mg N^{-1} m^{-3})	average diameter (m)	particle mass flux (kg/h)
1	87.00	1.10×10^{-6}	0.017545
2	145.44	1.10×10^{-5}	0.029263
3	153.60	3.10×10^{-5}	0.030904
3	146.24	5.10×10^{-5}	0.029423
4	100.16	7.10×10^{-5}	0.020152
5	87.20	9.10×10^{-5}	0.017545
6	13.28	1.11×10^{-4}	0.002672

To model the gas solid/liquid two-phase flow in the boiler, the gaseous phase was modeled in an Eulerian reference frame, whereas the discrete phase particles were modeled using the Lagrangian approach. The realizable version of the $k-\varepsilon$ model has been used for turbulence modeling. The Eddy dissipation concept (EDC) model is used for turbulence−chemistry interactions because it accounts for fine-scale turbulence structures with increased accuracy.[31] The stochastic tracking model (discrete random walk) was applied to predict the turbulent dispersion of ash particles. Radiation heat transfer between the particle and the furnace has been modeled with the discrete ordinates (DO) model.[30] All transport equations are solved with the segregated solver incorporating the SIMPLE algorithm for the coupling between the velocity and the pressure. Model convergence is determined when the residuals of the solution are smaller than the following orders of magnitude for the listed quantities: 10^{-6} for energy, 10^{-5} for species, 10^{-5} for continuity, and 10^{-6} for velocity. The procedure was modified by adding deposition growth formulas and variables in this work. As explained before, the deposition calculation is performed as a post-processor with all of the contributing factors obtained from the CFD calculations.

4.2. Gas Temperature and Condensation. The predicted gas temperature profile on the plane of symmetry of the boiler is shown in Figure 6a. The CFD simulation shows a

dx.doi.org/10.1021/ef201681t | Energy Fuels 2012, 26, 6501−6508

Table 4. Composition of Input for the CFD Model, with All Values in mol %

SO_2	SO_3	K	KO	KO_2	KOH	$K_2O_2H_2$	KCl	K_2Cl_2
3.59×10^{-4}	9.66×10^{-7}	4.39×10^{-9}	2.3×10^{-10}	6.5×10^{-10}	6.11×10^{-5}	2.41×10^{-10}	3.51×10^{-4}	3.39×10^{-6}
$KHSO_3$	KSO_4	KSO_2	KSO_3	$KHSO_4$	K_2SO_4	KSO_3Cl	$K_2SO_4[B]$	CO
4.79×10^{-10}	1.55×10^{-6}	7.19×10^{-11}	3.40×10^{-11}	1.16×10^{-11}	1.55×10^{-6}	9.49×10^{-11}	2.57×10^{-9}	3.68×10^{-8}
CO_2	H	O	OH	H_2	O_2	HO_2	H_2O	H_2O_2
0.153	6.99×10^{-9}	9.95×10^{-9}	3.39×10^{-6}	1.76×10^{-8}	3.10×10^{-2}	7.49×10^{-12}	0.11	8.49×10^{-12}
HOSO	$HOSO_2$	HCl	Cl_2	Cl	ClO	HOCl	ClOO	N_2
1.55×10^{-13}	9.88×10^{-12}	2.00×10^{-6}	7.79×10^{-12}	5.23×10^{-9}	5.59×10^{-13}	1.42×10^{-13}	4.60×10^{-11}	0.706

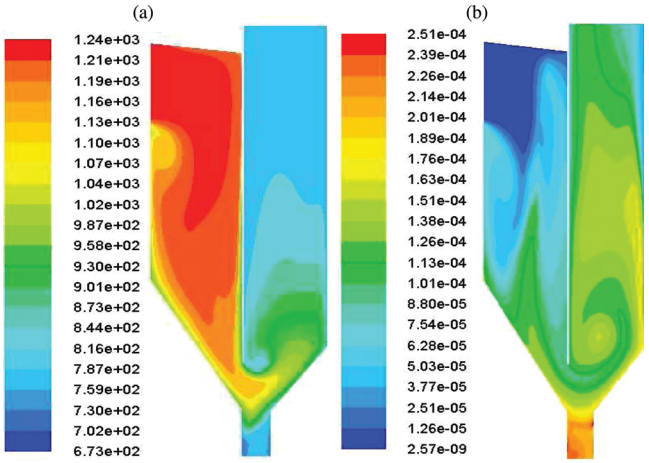

Figure 6. Contours of the (a) gas temperature (K) and (b) concentration field of $K_2SO_4[B]$ on the symmetry plane.

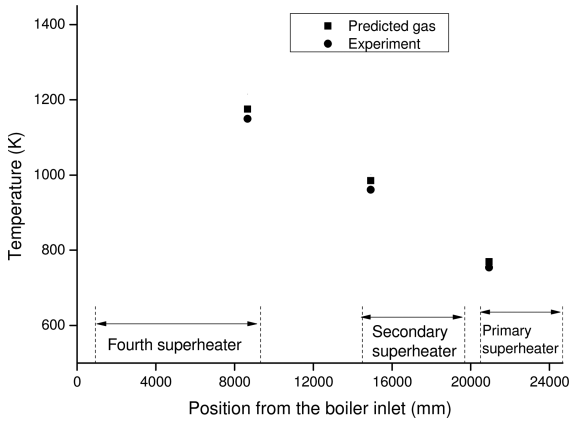

Figure 7. Measured gas and predicted gas temperature (K).

recirculation zone, with a very uneven distribution of the flue gas temperature. The initial drop in the temperature is due to the high heat-transfer rate to the water walls, particularly on the front wall just below the inlet (see Figure 6a). The subsequent fall in temperature over the height of the boiler is a result of the heat transfer to the secondary and primary superheaters.

Concerning the homogeneous alkali reactions, which involve the formation, nucleation, and condensation of salts, the formation of alkali sulfate in the gas phase and its subsequent condensation are the two main interests in this paper. However, a detailed modeling of the nucleation and condensation processes is not included in the present work. Instead, the effect of condensation is approximated by a second-order pseudo-reaction, with the rate constant being set to 10^{14} cm^3 mol^{-1} s^{-1}, as suggested by Glarborg et al.[8] to predicted the liquid-phase potassium sulfate $K_2SO_4[B]$. If the temperature is below 1240 K, condensed $K_2SO_4[B]$ is formed quickly.[8] However, we have followed the suggestion of the authors by setting the rate constant for the pseudo-reaction to 10^{13} cm^3 mol^{-1} s^{-1}, and the maximum $K_2SO_4[B]$ concentration can be found in the ash hopper, as shown in Figure 6b, and also further upstream over the height of the boiler.

Figure 7 shows the predicted gas temperatures in the region of the three superheaters compared to measured data. Experimental errors for the temperature measurements are approximately 5%. Therefore, the discrepancies observed in Figure 7 are believed to be reasonably small and satisfactory for the purpose of this investigation.

4.3. Gas and Particle Velocities. The motion of the particles caused by the mean gas velocity field can significantly influence the slagging pattern. It is usually assumed[16,35,36] that particles above 10 μm in diameter would be expected to make the largest contribution to the deposit formation on the front part of the heat exchangers in the convection section. Large particles above 10 μm in diameter hit the front part of the tube, while the particles smaller than 10 μm deposit on the side and rear parts of the tube mainly through thermophoresis or turbulent diffusion. Figure 8 shows the predicted particle, gas,

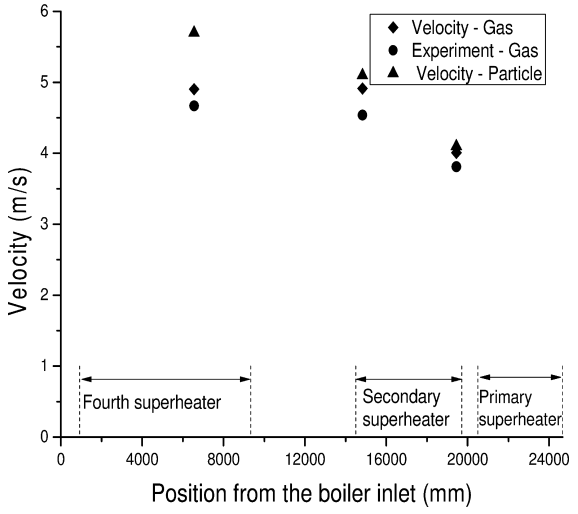

Figure 8. Measured gas and predicted gas and particle velocities.

and measured gas velocities at three locations, A, B, and C, close to the entrance/exit of the bundles of superheater tubes, as indicated in Figure 4. These particle velocities are magnitudes of the maximum velocities that were observed at these locations. Because of the complex interactions between the particles and superheater walls, as well as the complex gas flows and the effect of gravity, maximum velocity of the particles can be higher than the local averaged gas velocity.

dx.doi.org/10.1021/ef201681t | Energy Fuels 2012, 26, 6501–6508

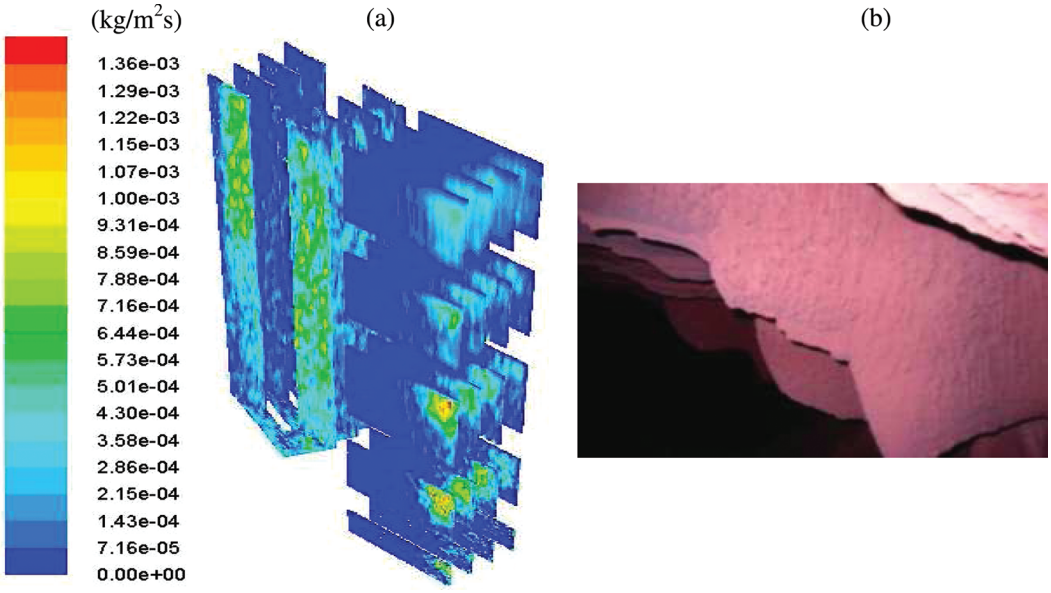

Figure 9. Deposit formation on the vertical surface of the superheaters: (a) predicted contour of the deposition rate in terms of the position and shape and (b) photo of the deposition formed on the vertical section of the secondary superheater (SH2).

The inertia of large particles is sufficient to allow for their trajectories to deviate from the mean gas streamlines close to the solid walls. In this region of the boiler, the gas velocity causes a stagnation of condensable species within the boundary layer of the tube, thus providing a sticking layer for the arriving particles. The predicted gas velocities on the vertical plane of the boiler are in good agreement with the measurement results. For the measurement points A and B, where velocities are relatively high, predictions are within an accuracy of about 5%.

4.4. Deposit Formation. The formation of the deposit of the ash particles has been calculated using the particle size dependence upon the ash-sticking probability in eq 1. The particles are assumed to be sticky if the sticking probability is greater than unity. Figure 9a shows the contour of the predicted deposition rates for a bank of 38 mm outside diameter (OD) pipes joined together. Estimated from the dimensions shown in Figure 4, the fourth, second, and first superheaters are located at approximately 8610, 15 210, and 22 100 mm from the boiler inlet, respectively. Because of the effect of the swirling flow downstream of the fourth superheater, particles are driven toward the second and first superheaters by centrifugal force. At the boundary layer of these superheaters, the temperatures are low and the impaction particles are captured by condensed potassium sulfates near the tube surface. However, some particles are only partially able to reach the primary superheaters located further upstream of the secondary superheaters; therefore, the deposit on it will develop slowly, as shown in Figure 9a. Detailed predictions of deposit formation on the rows of tubes have shown that the deposition rate on the first row of tubes exceeds that on the subsequent rows in the tube bank.[14,37] This decreasing rate of deposit formation on the row of tubes can be clearly seen on the front side of the first and subsequent tubes. The position of the deposits in Figure 9a has been guided by the contour map of K_2SO_4[B] formation, as shown in Figure 6b, particularly around SH2, where severity of the deposits have been reported experimentally by Niu et al.[34] and now validated by the model. In addition, the highest deposit location occurring at the right hand side on the secondary superheaters (SH2.2) illustrated in Figure 9b is adequately captured and easily noticeable on the secondary superheaters (SH2.2) in Figure 9a. This offers some evidence that the model has reproduced qualitative information regarding the deposition of fly ash with the thermal boundary layer on the surface of the superheater system. It should be noted, however, that the model is meant to predict the initial stages of deposition buildup assuming fresh and clean tube surfaces, while the experimental observation shown in Figure 9b is a result of continuous ash buildup, where the stickiness of the tube surface plays a significant role in the deposit accumulations on the heating surfaces.

5. CONCLUSION

A reduced alkali kinetic mechanism for alkali sulfate formation during biomass combustion has been developed from a detailed alkali mechanism. The reduced kinetic mechanism reproduces the alkali phenomena seen in experiments well over the range of operating conditions investigated. The agreement between experimental data and the model results shows that, while the reduced mechanism accurately reproduced the primary features of the detailed mechanism, both mechanisms compared favorably to the experimental data.

To predict the ash deposition, a deposition model has been developed. The model is based on the particle-sticking probability that takes into consideration the size of the ash particles, local vapor, and saturation pressure of the potassium salts, which determine the condensation of the salts on the particle surface. The deposition model developed, together with the reduced alkali kinetic mechanism, was implemented into a multi-dimensional CFD model. The integrated model has qualitatively reproduced the key deposit positions as observed experimentally in the large-scale industrial boilers investigated firing cotton straw. Further work will consider the installation of a well-controlled ash deposition probe to obtain the actual deposition flux and to verify the model quantitatively.

AUTHOR INFORMATION

Corresponding Author

*E-mail: l.ma@leeds.ac.uk.

Notes

The authors declare no competing financial interest.

■ ACKNOWLEDGMENTS

M. U. Garba acknowledges the financial support of the Nigerian Government provided through the Overseas Scholarship Scheme of the Petroleum Technology Development Fund. The authors acknowledge the Shanyang Power Plant, China, for providing the experimental test facility. The authors thank the Engineering and Physical Sciences Research Council (EPSRC) (EP/F061188/1) for the financial support for this work.

■ NOMENCLATURE

C_p = concentration of fly ash particles (mg N^{-1} m^{-3})
$C_{t,p}$ = total concentration of fly ash particles (mg N^{-1} m^{-3})
D_i = diffusion coefficient of the ith gaseous component through the flue gas (m^2/s)
d_p = ash particle diameter (μm)
k = Boltzmann's constant (kg m^2 s^{-2} K^{-1})
$\dot{m}$ = mass flux of solid particles (kg m^{-2} s^{-1})
$m_{c,A}$ = flux of ash vapors (kg m^{-2} s^{-1})
$m_{trj,i}$ = mass flux of the particles (kg m^{-2} s^{-1})
P = sticking probability
p_i = partial pressure of the ith gaseous component (Pa)
$p_{s,i}$ = saturation pressure of the ith gaseous component at the surface temperature (Pa)
Sh = Sherwood number
T_f = flue gas temperature (K)
T_p = particle temperature (K)

Subscripts

A = surface area
c = condensing ash vapor
f = flue gas
p = particle
s = saturation
t = total
trj = trajectory

Symbols

[B] = condensed form
ρ = gas density (kg/m^3)
πd_p^2 = spherical surface area (m^2)

■ REFERENCES

(1) Junfeng, L. *Appl. Energy* **1997**, *56* (3/4), 381−394.
(2) Palz, W.; Coombs, J.; Hall, D. O. *Energy from Biomass: 3rd E.C. Conference*; Taylor and Francis Group: Abingdon, U.K., 1985; pp 369−375.
(3) Baxter, L. L. *Biomass Bioenergy* **1993**, *2*, 85−102.
(4) Kaer, S. K. Numerical investigation of deposit formation in straw-fired boilers. Ph.D. Thesis, Aakborg University, Aalborg, Denmark, 2001; pp 30−35.
(5) Kaer, S. K. *Fuel* **2004**, *83*, 1183−1190.
(6) Kaer, S. K. *Proceedings of the First Biennial Meeting of the Scandinavian−Nordic Section of Combustion Institute*; Gothernburg, Sweden, April 18−20, 2001; pp 91−96.
(7) Glarborg, P.; Marshall, P. *Flame* **2005**, *141*, 22−39.
(8) Hindiyarti, L.; Frandsen, F.; Livbjerg, H.; Glarborg, P. *Fuel* **2008**, *87*, 1591−1600.
(9) Jiménez, S.; Ballester, J. *Fuel* **2007**, *86*, 486−493.
(10) Jensen, J. R.; Nielsen, L. B.; Schultz-Møller, C.; Wedel, S.; Livbjerg, H. *Aerosol Sci. Technol.* **2000**, *33*, 490−509.
(11) Christensen, K. A.; Stenholm, M.; Livbjerg, H. *J. Aerosol Sci.* **1998**, *29* (4), 421−444.
(12) Kassman, H.; Bäfver, L; Åmand, L. E. *Combust. Flame* **2010**, *157*, 1649−1657.
(13) Christensen, K. A.; Livbjerg, H. *Aerosol Sci. Technol.* **2000**, *33*, 470−489.
(14) Boonsongsup, L.; Iisa, K.; Frederick, W. J. *Ind. Eng. Chem. Res.* **1997**, *36*, 4212−4216.
(15) Iisa, K.; Lu, Y. *Energy Fuels* **1999**, *13*, 84−90.
(16) Tomeczek, J.; Palugniok, H.; Ochman, J. *Fuel* **2004**, *83*, 213−221.
(17) Forstner, M.; Hofmeister, G.; Joller, M.; Dahl, J.; Braun, M.; Kleditzsch, S.; Scharler, R.; Oberberger, I. *Prog. Comput. Fluid Dyn.* **2006**, *6* (4/5), 248−261.
(18) Akbar, S.; Schnell, U.; Scheffknecht, G. *Combust. Theory Modell.* **2010**, *14* (3), 315−329.
(19) Ma, L.; Pourkashanian, M.; Williams, A.; Jones, J. M. *Proceeding of the American Society of Mechanical Engineers (ASME) Turbo Expo: Power for Land, Sea, and Air Conference*; Barcelona, Spain, May 8−11, 2006.
(20) Huang, L. Y.; Norman, J. S.; Pourkashanian, M.; Williams, A. *Fuel* **1996**, *75* (3), 271−279.
(21) Degereji, M. U.; Ingham, D. B.; Ma, L.; Pourkashanian, M.; Williams, A. *Fuel* **2011**, DOI: 10.1016/j.fuel.2010.12.038.
(22) Tomeczek, J.; Wacławiak, K. *Fuel* **2009**, *88*, 1466−1471.
(23) Bryers, R. W. *Prog. Energy Combust. Sci.* **1996**, *22* (1), 29−120.
(24) Kee, R. J.; Rupley, F. M.; Meeks, E. *Chemkin III: A FORTRAN Chemical Kinetics Package for the Analysis of Gas Phase Chemical and Plasma Kinetics*; Sandia National Laboratories: Livermore, CA, 1996.
(25) http://garfield.chem.elte.hu/Combustion/kinalc.htm.
(26) Turányi, T.; Bérces, T.; Vajda, S. *International Journal of Chemical Kinetics* **1989**, *21*, 83−99.
(27) Fluent Europe. *FLUENT User's Guide, Version 6.3*; Fluent Europe Limited: Sheffield, U.K., 2006.
(28) Venturini, P.; Borello, D.; Iossa, C.; Lentini, D.; Rispoli, F. *Energy* **2010**, 3008−3021.
(29) Zhou, H.; Jensen, P.; Frandsen, F. *Fuel* **2007**, *86*, 1519−153.
(30) Ma, L.; Gharebaghi, M.; Porter, R.; Pourkashanian, M.; Jones, J. M.; Williams, A. *Fuel* **2009**, *88*, 2448−2454.
(31) Magnussen, B. F.; Hjertager, B. H. *Proc. Int. Combust. Symp.* **1976**, 719−729.
(32) Shin, D.; Choi, S. *Combust. Flame* **2000**, *121*, 167−180.
(33) www.factsage.com.
(34) Niu, Y.; Tan, H.; Ma, L.; Pourkashanian, M.; Liu, Z.; Liu, Y.; Wang, X.; Liu, H.; Liu; Xu, T. *Energy Fuels* **2010**, *24*, 5222−5227.
(35) Walsh, P. M.; Sayre, A. N.; Loehden, D. O.; Monroe, L. S.; Beer, J. M.; Sarofim, A. F. *Prog. Energy Combust. Sci.* **1990**, *16*, 327−346.
(36) Obernberger, I.; Brunner, T.; Jöller, M. *Proceedings of the IEA-Seminar "Aerosols from Biomass Combustion"*; Nussbaumer, T., Ed.; Verenum: Zürich, Switzerland, 2001; pp 69−74.
(37) Weber, R.; Mancini, M.; Schaffel-Mancini, N.; Kupka, T. *Fuel Process. Technol.* **2011**, DOI: 10.1016/j.fuproc.2011.09.008.